

Comparative tests on the performance of solar stills enhanced by pebbles, corrugated plate and membrane distillation and construction of performance prediction model for rock type still

Lu Zuo[*, a], Chenkai Xiao[b], Ziyang Yan[c], Zinan Guo[a], Long Huang[a], Yunting Ge[d]

[a] College of Renewable Energy, Hohai University, Changzhou, China

[b] School of Electrical and Power Engineering, Hohai University, Nanjing, China

[c] NR Electric Co., Ltd, Nanjing, China

[d] School of the Built Environment and Architecture, London South Bank University, London, UK

Abstract: To improve the water production capacity of solar still (SS), realize the theoretical prediction of the enhanced SS performance, and enrich the theoretical research basis of the desalination technology of SS, this paper sets up three kinds of enhancement measures, namely, rock, corrugated plate and membrane distillation, tests the enhanced water production effect, and reveals the enhanced operation mechanism. At the same time, a performance prediction model of rock enhanced was established based on the body-centered cubic stacking rock technology, and the influence of rock parameters on the distillation effect was studied. The study found that the water production increment of the three enhancement measures was concentrated in the rising period of the water production of the SS, and the total water production was 6.38%, 12.30% and 11.63% higher than that of the traditional basin SS, respectively. The rock or corrugated plate enhances the distillation effect by elevating the seawater temperature and its temperature difference with the cover plate, and the membrane distillation increases the total water production through the additional water production of the membrane. Moreover, the constructed model can effectively predict the characteristics of rock enhanced SS. The increase in the rock layer thickness and the decrease in the rock particle size and material heat capacity both enhance the total daily water production, but the effect of rock particle size and material is weak. Although the increase of thickness increases the water production obviously, it aggravates the fluctuation of water production.

Keywords: Seawater desalination; Solar still; Rock enhanced; Membrane distillation enhanced;

[*] Corresponding author.

E-mail address: zuoluhhu@163.com (L. Zuo).

Corrugated plate enhanced;

Nomenclature

A	area, m^2
C_p	specific heat, J/(kg·K)
g	gravitational acceleration, 9.8 m/s^2
G	solar irradiance, W/m^2
h_c	convective heat transfer coefficient, $W/(m^2 \cdot K)$
h_e	evaporation heat transfer coefficient, $W/(m^2 \cdot K)$
h_r	radiation heat transfer coefficient, $W/(m^2 \cdot K)$
M	mass per unit area, kg/m^2 or hourly water production
p	pressure, Pa
q	heat flux, $W/(m^2 \cdot K)$
r	radius, m or correlation coefficient
T	temperature, K
v	velocity, m/s
Subscripts	
a	ambience
air	air
b	bottom plate
gc	glass cover
ins	insulation layer
s	sky
hss	heat storage surface
hs	heat storage
sw	seawater
wind	ambient wind
Greek Symbols	
σ	Boltzmann constant, 5.67×10^{-8} $W/(m^2 \cdot K^4)$
ε	emissivity
α	absorptivity
τ	transmissivity or time
λ	thermal conductivity, W/(m·K)
δ	thickness, m
ρ	density, kg/m^3
μ	dynamic viscosity, kg/(m·s)
ν	kinematic viscosity, m^2/s
ϕ	porosity
η	efficiency, %
Dimensionless number	
Nu	Nusselt number

Ra	Rayleigh number
Re	Reynolds number
Pr	Prandtl Number

1. Introduction

Solar energy is the only heat source for traditional solar still (SS). Although solar energy is a resourceful, clean and safe energy, it is an intermittent and unstable energy source. SS for seawater desalination requires a large evaporation area, with low water production per unit area and low efficiency. Therefore, how to increase the water production of SS has become the focus of scholars' research.

There are some scholars who have improved the absorption rate and water production of SS by improving the material [1], geometry [2] and internal structure [3] of SS. Some scholars innovatively combined membrane distillation modules with SS to produce water by utilizing membrane distillation principle and SS principle together. Shirsath et al. [4] explored the water production performance of SS with surface-mounted hydrophobic membrane. The results showed that the water production of SS could be increased by 40-70% with the addition of membrane modules. Zuo et al. [5] proposed a novel membrane distillation enhanced disc solar still by installing an air-gap membrane module vertically in the SS. The membrane module, which is less than one-seventh of the evaporation area of the disc evaporation area, can increase the daily water production of SS by 7.6%.

Many other scholars have chosen to add heat storage materials to the SS. This is because heat storage materials can store energy during sunlight and act as a heat source to release energy to increase freshwater production during the sunless period. According to the heat storage mode, heat storage materials can be divided into three types: latent heat storage, sensible heat storage and thermochemical heat storage [6]. Among them, phase change materials are a good latent heat storage material used to increase the water production of SS [7], while sensible heat storage materials are widely used in SSs due to their relatively simple storage and release processes, convenient use and low cost. There are many studies in this area.

Karthick et al. [8] used Omani rock as a heat storage medium in a SS. A comparative analysis with the conventional SS operation test experiment showed that the water production of the SS was increased by 18.6% after laying the rock stone bed. Abdel-Rehim et al. [9] laid a heat storage layer consisting of glass balls with a diameter of 13.5 mm in a conventional SS. Experimental study showed that the efficiency of the modified SS increased by 5%, 6% and 7.5% in the months of May, June and July, respectively. Nafey et al. [10] tested using 10 mm thick black rubber material and 20-30 mm particle size black gravel in a conventional SS and found that the water production of the SS increased by 20% and 19% respectively. In addition, the black gravel absorbed and released solar radiant energy faster than that of black rubber. Murugavel et al. [11] tested the performance of the system after using different sizes of quartzite rock, red brick pieces, cement concrete pieces, washed stones, iron scraps, and other sensible heat storage materials in a double slope SS. The results showed that 3/4-inch quartzite had the best enhanced of water production in SS. Gnanaraj et al. [12] divided the bottom plate of SS into 25 sections and scattered five types of heat storage materials in them simultaneously with black granite blocks, red brick blocks, pebbles, charcoal and sand. The experimental results showed that the water production of the SS with heat storage materials increased by 23.08% compared to that of the conventional SS, and at the same time, the SS with heat storage materials was able to maintain a higher water temperature and water production in the case of reduced sunlight hours. Sakthivel et al. [13] used 6 mm grain size black granite as a thermal storage material to experimentally investigate the effect of rock heat storage material on the performance of SS at different rock layer thicknesses. In addition, a mathematical model was developed to simulate the actual experimental results and it was found that the simulated and actual values were in good agreement. Abdallah et al. [14] added black volcanic rock to SS to improve the thermal performance and increase the freshwater yield of a conventional SS. The experimental results showed that the freshwater gain from the addition of black volcanic rock was about 60% and there was no corrosion problem. Arjunan et al. [15] used various heat storage materials such as black granite gravels, pebbles, and blue metal stones in their experiments, and the results showed that the water production in SS at night increased significantly with the use of heat storage materials, and that the heat storage properties of black granite gravels were better than those of pebbles and blue metal stones. Rajaseenivasan et al. [16] placed charcoal, sand and metal scrap as heat storage materials in the spaces between rectangular glass fins on the bottom plate of SS and water production increased by 33.7%, 26.74% and 29.3%, respectively. Gnanaraj et al. [17] laid black granite of 10-15 mm particle size at the bottom of a conventional double slope SS, which significantly increased the water production in the afternoon and at night in the distillation tank, with a 69.84% improvement in daily water production at the same water level. Madhu et al. [18]

experimental study found that the use of rubber mat and polyester mat in SS increased the water production of the SS by 57.1% and 59.5% respectively. Bilal et al. [19] tested the use of pumice stones as heat storage material under the same water quantity conditions and found that the daytime water production of SS decreased by 10.35% and 17.02% and nighttime water production increased by 1.32% and 3.62% when 5 kg and 10 kg of pumice stones were used, respectively, and the daily water production decreased with the increase in the mass of the stones. Patel et al. [20] used Thermic fluids HP-500 as a heat storage material in a conventional SS and it was found that at a water depth of 2 cm, there was an increase of 11.24% in the water production of the SS. Kabeel et al. [21] used jute cloth knitted with sand as heat storage material. The sand continuously releases the stored heat and evaporates the moisture absorbed by the jute cloth. Also due to the capillary action and water absorption of the jute cloth, the evaporation of water can be accelerated. It was found that the water production of SS increased from 5.5 kg/m^2 to 5.9 kg/m^2. Kabeel et al. [22] investigated the performance of SS with high thermal conductivity graphite as absorber plate and heat storage material at the same water level. The experimental results showed that the daily water production was enhanced by 74.89% to 80.05% by using graphite. Omara et al. [23] experimentally investigated the effect of yellow and black sand beds on the thermal performance of SS. The results showed that the daily water production increased by 42% and 17% with the use of black and yellow sand beds, respectively. Samuel et al. [24] encapsulated 127 g of rock salt in spheres made of plastic with a diameter of about 6 cm and arranged several such spheres on the bottom plate of a SS as heat storage material. It was found that the daily water production of SS increased from 2.6 kg/m^2 to 3.7 kg/m^2. Kumaravel et al. [25] used blue metal stones and pebbles to store heat in SS. The experimental results showed that the enhanced of water production in the SS by metal stones was better than that of pebbles; and the freshwater production increased by 18% in the SS using both metal stones and pebbles as compared to that of the conventional SS. Prasad et al. [26] added black-painted copper plate and phosphate pellets as heat storage material in a conventional SS. The experimental results showed that the water production increased by 14.96% when black-painted copper plate was used alone and by 29.53% when a combination of copper plate and phosphate pellets was used. Saravanan et al. [27] used marble as heat storage material in a dual slope SS and found that the daily water production of the SS was increased from 3.52 L/m^2 to 4.094 L/m^2 and the efficiency of the system was increased by 16.32%. Dumka et al.

[28] added cotton bags filled with sand to the conventional SS to increase the heat storage capacity and water surface area. The cumulative water production of the SS was increased by 28.56% and 30.99% with 30 kg and 40 kg basin water, respectively, and the overall efficiency of the system was increased by 28.96% and 31.31%, respectively. Mohamed et al. [29] experimentally evaluated the enhanced of black basalt on the performance and freshwater production of SS. The results showed that the water production of the SS was enhanced by 19.81%, 27.86% and 33.37% for 1 cm, 1.5 cm and 2 cm stone sizes, respectively; and the maximum daily thermal efficiency of the SS was about 22.6% for 2 cm stone size, which is an improvement of about 32.07%. Attia et al. [30] used salt balls as heat storage materials in hemispheric solar distillatory. Four different sizes of spherical rock salt balls (0.50, 1.0, 1.50 and 2.0 cm) were tested, and it was found that the water yield was 45.6 %, 34.4 %, 27.3 % and 21.9 % higher than that of the reference hemispheric solar distillatory, respectively.

Currently, the more widely used sensible heat storage materials in SS are locally available and inexpensive rock materials of various types, and the use of these rock materials has considerable enhanced effects on the thermal performance and freshwater output performance of the SS. However, most of the existing studies on rock heat storage to enhance the performance of SS are mostly limited to experimental studies, and the theoretical studies are very few, which are unable to carry out theoretical simulation and prediction of the operational characteristics of the SS as well as the optimization of the heat storage material configuration. In order to enhance the water production capacity of SS, realize the theoretical prediction of the enhanced SS performance, and enrich the theoretical research basis of the desalination technology of SS, based on the experimental test, this paper makes a horizontal comparative study on the effects of rock, corrugated plate and membrane distillation enhancement measures, and tests their operation rules and water production effects to reveal the enhanced operation mechanism and provide data support for theoretical research. At the same time, a non-stationary physical mathematical model of rock enhanced SS is established based on the body-centered cubic stacking rock technology to realize the function of theoretical simulation, prediction and optimization of the operating characteristics of rock enhanced SS. Relying on the constructed mathematical model, the influence of rock parameters on the distillation effect is investigated, and the optimized configuration of rock materials is carried out to further enhance the performance of SS.

2. Construction of solar still enhanced by different technologies

The experimental setups of different technologies enhanced SS are shown in Fig. 1. In Fig. 1(a) from back to front are the traditional basin solar still (SS1), rock enhanced solar still (SS2), corrugated plate enhanced solar still (SS3) and membrane distillation enhanced solar still (SS4), respectively. The four stills are identical in structure and size, and their geometric dimensions are shown in Fig. 1(b). 8 mm thick plexiglass is used for the bottom and walls of the stills. The bottom surface and inner side walls of the basin are painted black. The outside surface of the bottom and wall paste 20 mm-thick black rubber-plastic board, and then lay 30 mm-thick polystyrene foam board. A 3.5 mm thick transparent plate glass is used for the cover of the still. The seawater in the basin is simulated by sea crystal and the seawater depth in each SS was 10 cm.

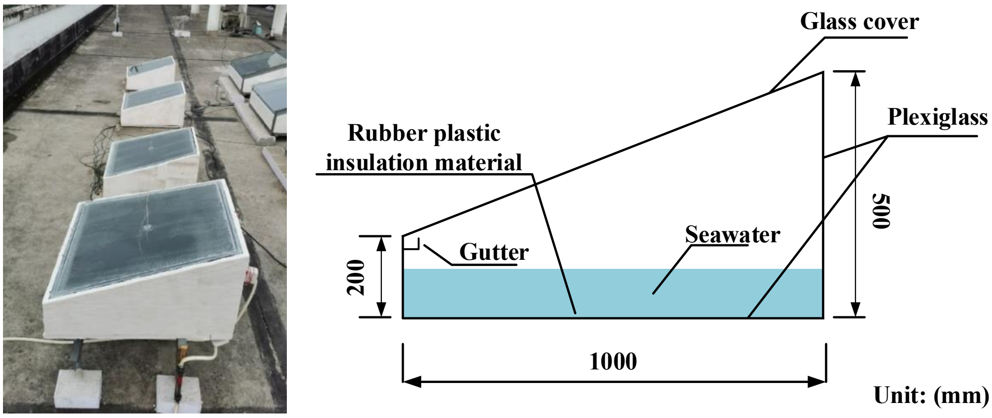

(a) Experimental setups **(b) Geometric dimensions**

Fig.1. The experimental setups of different technologies enhanced SS

The rocks used in the SS are shown in Fig. 2 as flat black and gray pebbles, and their heat storage layer parameters and physical properties are shown in Table 1. The rocks were uniformly laid and spread over the bottom plate in the SS to form the rock heat storage layer, which was about 4.0 cm thick. The physical drawing and corresponding dimensions of the corrugated plate used in the SS are shown in Fig. 3. The corrugated plate is made of black and gray plexiglass and is designed with 5 equally spaced tabs with a width of 10 cm, a height of 4 cm and a groove width of 10 cm. The corrugated plate is arranged over the bottom plate of the SS.

Fig. 2. Pebbles

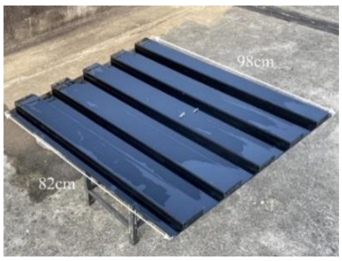

Fig. 3. Physical drawing and dimensions

Table 1 Parameters and physical properties of pebble heat storage layer

Parameters and physical properties	Value
Average thickness	1.8 cm
Average horizontal particle size	5 cm
Density [25]	2563 kg/m^3
Thermal conductivity [25]	2.07 W/(m·K)
Specific heat capacity [25]	820 J/(kg·K)

The membrane module was installed vertically on the high side of the still, as shown in Fig. 4, with a length of 83 cm, a height of 10 cm, and a width of 6 cm. The area of the hydrophobic microporous membrane is 2×36×6 cm^2, the thickness is 160 μm, the membrane pore size is 1.2 μm, the membrane porosity is 0.8, the membrane tortuosity is 2, and the membrane thermal conductivity is 0.25 W/(m·K). The thickness of the air gap between the hydrophobic microporous membrane and the condensation plate is 5 mm. The condensation plate is made of plexiglass, and the cooling water is tap water, which enters the condensation room from the lower part of the condensation room by the introduction water pipe. Under the action of tap water pressure, the cooling water flows upwards in the condensation room while absorbing the condensation latent heat released by the condensation of water vapor in the membrane module on the condensation plate, and then flows out from the outlet pipe on the top side wall of the condensation room. The water flow rate is 200 L/h and is set by means of a float flow meter.

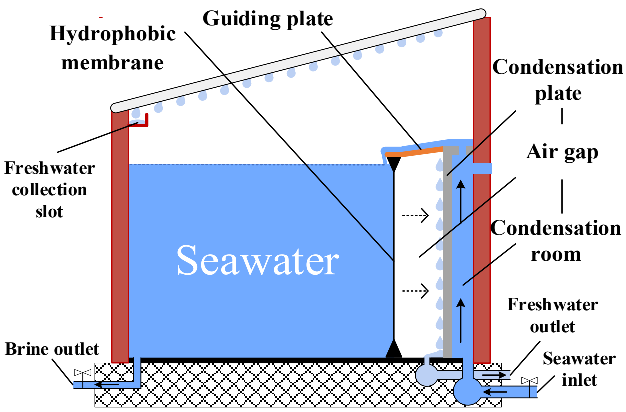

Fig. 4. Vertical installation of membrane module

Solar irradiance, ambient temperature and humidity, and ambient wind speed were measured by photoelectric solar radiation sensor, temperature and humidity transmitter and three-cup wind speed sensor respectively. Platinum resistance was selected to measure the internal and external surface temperature of the cover, seawater temperature and cooling water temperature. The details of the sensors are listed in Table 2. Solar irradiance, ambient temperature and humidity, ambient wind speed and temperature of each measurement point of the still were automatically collected by the measurement system with an interval of 5 min. Fig. 5 shows the arrangement of the temperature measurement points of the four stills and the composition of the collection system.

Table 2 Sensor information

Equipment	Model	Range	Accuracy and error
Photoelectric solar radiation sensor	RS-RA-*-JT	0~1800 W/m^2	1 W/m^2, ±2%
Temperature and humidity transmitter	RS-WS-N01-SMG	−40 °C~+120 °C 0% RH~80% RH	±0.5 °C, (25 °C) ±3% RH
Three-cup wind speed sensor	RS-FSJT-*	0~30 m/s	±(0.2+0.03V) m/s
Platinum resistance temperature sensor	WZP-PT100	−40 °C~+200 °C	±(0.15+0.002T) °C

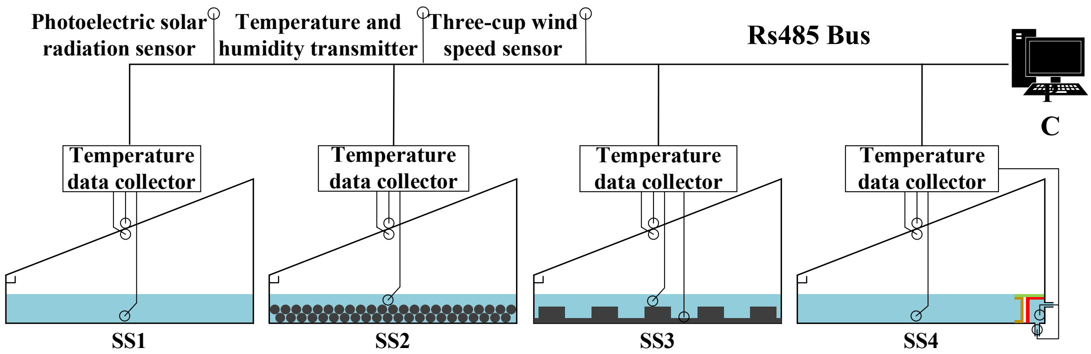

Fig.5. Measurement points arrangement and acquisition system composition

The freshwater produced by each SS flowed into a 500 ml mineral water bottle through a drainage tube and was weighed every 60 min by an electronic scale with a range of 0-5000 g and an accuracy of 1 g. After recording the water production data, the freshwater was poured back into the still through the water level indicator channel leading from the side wall of the SS to keep the brine concentration and the thickness of the seawater layer unchanged.

The test site is the roof of the Qinxue Building of Jiangning Campus of Hohai University in Nanjing (31°54′50″N 118°47′10″E). After the stable operation of the device, the test data collection began at 09:00 a.m. on September 8, 2021 and ended at 11:30 a.m. on the 9th.

3. Results and discussion

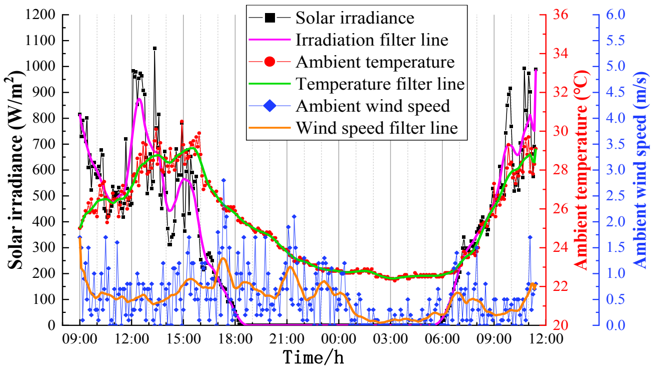

Fig.6. Solar irradiance, ambient temperature and ambient wind speed conditions

Fig. 6 shows the curves of solar irradiance, ambient temperature and ambient wind speed on the test day, from which it can be seen that the test day is representative of the sunny weather in autumn.

Fig. 7 shows the temperature variation curves of each measuring point in the four stills under the same seawater level, and Fig. 8 shows the temperature difference between the seawater and the inner surface of the cover in the four stills under the same seawater level. As can be seen from Fig. 7, the change trend of seawater temperature in the four stills was the same, only the values were different. From an overall perspective, SS3 had the highest seawater temperature. The seawater temperature at SS2 was lower than that at SS3 for most of the time, except for the time period in the area of peak seawater temperature, which was slightly higher than that at SS3. The seawater temperatures in both SS2 and SS3 were slightly higher than those in SS1 as a whole, and significantly higher in the peak region than those in SS1. The peak seawater temperatures in SS3 and SS2 were 47.3°C and 47.5°C, respectively, which were 1.2°C and 1.4°C higher than those in SS1, respectively. This is because the laying of corrugated plate and rocks at the same water level makes the seawater in the stills less voluminous and less thermally inert, so the seawater heats up faster and rises higher. In addition, the presence of black and gray corrugated plate and rock heat storage reduces the reflectivity of the bottom of the still, which can absorb more solar radiation and reduce the preheating time of the seawater, shortening the seawater heating time and thus increasing the temperature difference with the glass cover. It can also be seen from Fig. 8 that the seawater-cover temperature difference under these two enhancements was slightly higher than that of the traditional one. The increase of seawater temperature and seawater-cover temperature difference will promote the evaporation and condensation of seawater, which is conducive to the increase of freshwater production.

These also fully indicate that the corrugated plate and rocks have the effect of improving the heat storage effect of traditional SS. Since the corrugated plate has a larger surface area to receive solar radiation, which means that it can absorb more solar energy, the corrugated plate is more effective in improving the heat storage effect of the SS than the rocks.

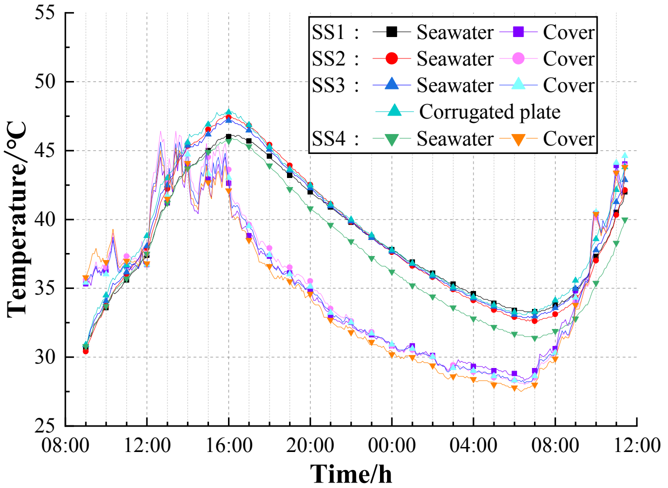

Fig.7. Temperature variation curve

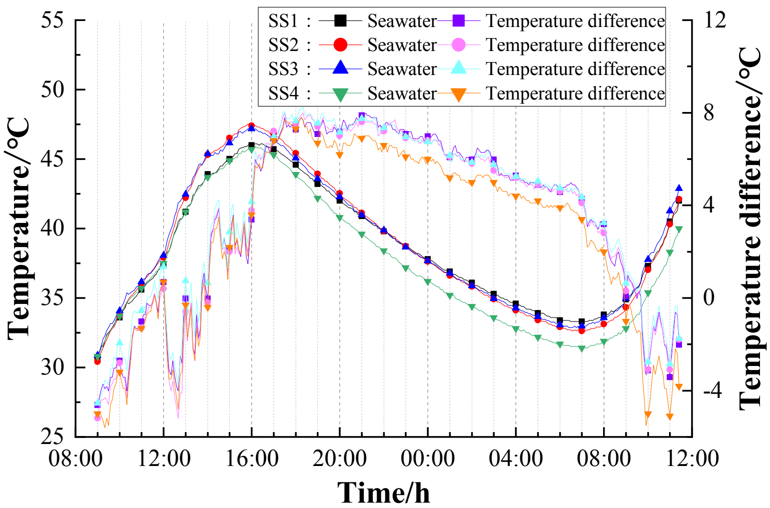

Fig.8. Temperature difference curve

As can be seen in Fig. 7, SS4 had the lowest seawater temperature and it was significantly lower than that of the other three units. According to the literature [5], the membrane distillation enhanced only additionally adds the membrane distillation effect to water production, but does not improve the heat storage effect of the still. In addition, due to the design limitations of the experimental device, the latent heat of condensation released by the condensation of the water vapor in the membrane module is absorbed by the cooling water in the condensation room. As the cooling water is discharged away, the latent heat is not recycled. So, it exacerbates the heat loss from the still to the outside world, making the seawater temperature significantly lower than that of the other three. This also indicates that it is important to recover the latent heat of condensation released on the condensing plate back into the SS.

It can also be seen from Fig. 7 that the four SSs have the same trend of cover temperatures with very small differences. The seawater temperature of the SS enhanced by membrane distillation is significantly lower than the seawater temperature of the other three units, and its cover temperature is slightly lower than that of the other three units, so its seawater-cover temperature difference is lower than that of the other three units, as shown in Fig. 8.

It can also be seen from Fig. 7 that for the corrugated plate enhanced SS, the temperature change of the corrugated plate bottom plate is similar to that of its seawater temperature. Only in the sunshine period, the temperature of the corrugated plate is significantly higher than the seawater temperature, while there is no difference with the seawater temperature in other periods. This is because the black corrugated plate can receive more solar radiation through the glass cover and seawater layer during the sunshine period, which improves the utilization rate of solar energy. The base of the corrugated plate is thinner, and under the same irradiance, the bottom plate warms up faster than the convex platform, and because seawater warms up mainly by absorbing the heat transferred from the bottom plate and the convex platform, the temperature of the bottom plate is significantly higher than that of the seawater. The corrugated plate is used as an exothermic source to heat the seawater in other time periods, and with the output of the heat source, the temperature of the corrugated plate itself decreases, and finally it is basically the same as the seawater temperature.

From the overall view of the change curves in Fig. 8, the seawater-cover temperature difference was the highest under corrugated plate enhanced. The seawater-cover temperature difference under rock enhanced had little difference with that of the traditional SS, and the seawater-cover temperature difference under membrane distillation enhanced was the lowest. Since the environmental conditions above the glass cover are the same, the change in seawater-cover temperature difference under the same heat dissipation conditions is mainly related to the amount of convective heat transfer between the seawater and the glass cover, and thus depends more on the change in seawater temperature.

Fig. 9 shows the variation curve of the hourly freshwater production of the four stills at the same seawater level. As can be seen, the peak water production areas of the four units were all around 18:00. In the rising period of water production, the water production of the enhanced still was higher than that of the traditional still. Because at this stage, the positive temperature difference is the main factor affecting the water production rate [31]. In the peak water production area, the water production of the enhanced still was much higher than that of the traditional still, because the seawater temperature is much higher than 40°C at around 18:00, with a large seawater-cover temperature difference and strong seawater evaporation power. During this period, the seawater temperature under corrugated plate enhanced and rock enhanced was significantly higher than that in traditional still, and the temperature difference between seawater and glass cover was also higher than that in traditional still. In the period of decreasing water production, the difference between the water production of the enhanced still and the traditional still is very small. Because seawater temperature is the main factor affecting water production at this stage [31], the difference between seawater temperature under corrugated plate enhanced and rock enhanced is very small compared with that of traditional still.

The freshwater production under membrane distillation enhanced in Fig. 9 consists of two parts, namely the hourly water production of basin distillation and membrane distillation. Although the seawater temperature and seawater-cover temperature difference of the SS4 are the lowest among the four stills, which means that the basin distillation water production in SS4 determined by these two factors is lower than that of other stills, the total hourly water production of SS4 is instead superior to that of SS2 because it is compensated by the membrane distillation water production.

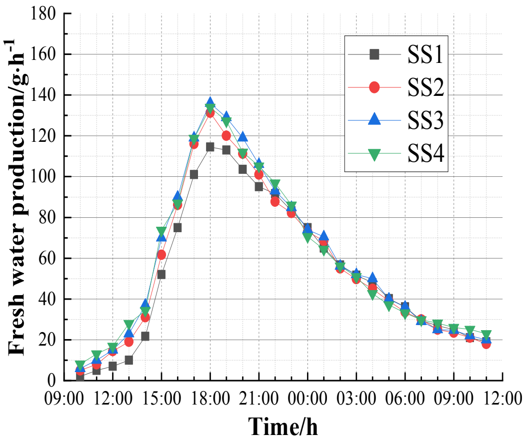

Fig.9. Hourly water production

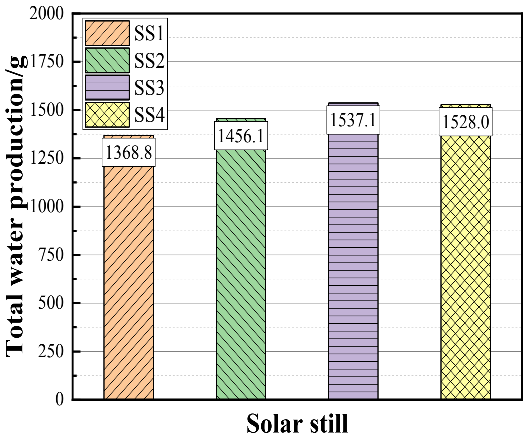

Fig.10. Total water production

Fig. 10 shows a histogram of the total water production of the four stills during the test period at the same seawater level. It can be seen from the figure that these enhanced processes can increase freshwater production, and the corrugated plate enhanced has the best effect, followed by membrane distillation enhanced and rock enhanced. During the whole test period, the total water production of rock enhanced, corrugated plate enhanced and membrane distillation enhanced stills increased by 6.38%, 12.30% and 11.63%, respectively, compared to that of the traditional still.

4. Construction and validation of a model for predicting the performance of a rock enhanced solar still

4.1 Predictive model construction for performance of rock enhanced solar still

Fig. 11 shows a physical model of a rock enhanced SS. In the still, a rock heat storage is laid on the floor of the still. During the period of solar irradiation, the surface layer of the rock heat storage absorbs the solar radiation through the glass cover and heats up, and part of the heat stored in the surface layer is used to heat the seawater above it, and part of it is transferred to the heat storage layer below for storage. During periods of no solar irradiation, the heat stored in the rock heat storage begins to be released to heat the seawater.

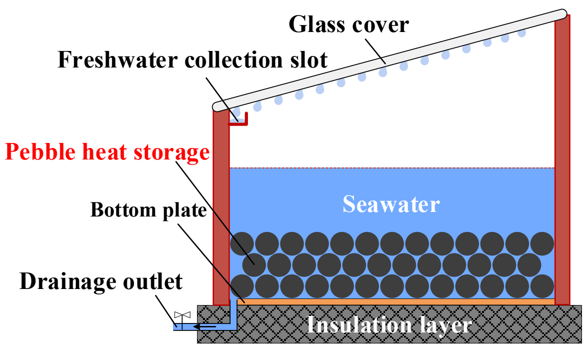

Fig.11. Physical model of a rock enhanced SS

In order to theoretically calculate and predict the freshwater production of the rock enhanced SS and find ways to improve its performance, it is necessary to construct a mathematical model of energy transfer, and analyze and comprehensively study the heat and mass transfer processes in the still. In order to facilitate the further development of the study, the following assumptions are made:

① Ignoring the temperature difference in the glass cover, it is approximated as a lumped heat capacity.

② Ignoring the temperature difference in the seawater layer, it is approximated as a lumped heat capacity.

③ Ignoring the temperature difference in the bottom plate, it is approximated as a lumped heat capacity.

④ Ignore differences in solar irradiation angles.

⑤ The sealing and heat preservation performance of the still is good, and there is no steam leakage.

⑥ The shape of the rock is approximately equal-diameter sphere, and the sphere is arranged in a body-centered cubic stacking mode.

The energy transfer process in the rock enhanced SS is shown in Fig. 12.

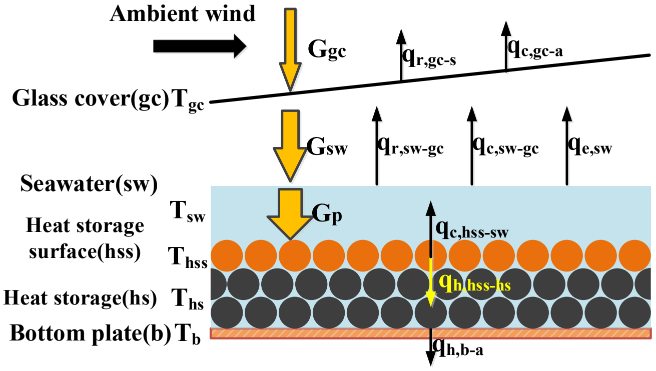

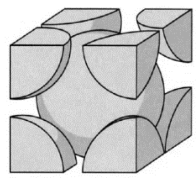

Fig.12. Energy transfer process in rock enhanced SS Fig.13. Body-centered cubic stacking mode

(1) The heat balance equation of the glass cover is:

$$\alpha_{gc}G+q_{r,sw\text{-}gc}+q_{c,sw\text{-}gc}+q_{e,sw}=q_{r,gc\text{-}s}+q_{c,gc\text{-}a}+C_{p,gc}M_{gc}\frac{\mathrm{d}T_{gc}}{\mathrm{d}\tau} \tag{1}$$

Radiative heat transfer rate between seawater and glass cover $q_{r,sw\text{-}gc}$:

$$q_{r,sw\text{-}gc}=h_{r,sw\text{-}gc}\left(T_{sw}-T_{gc}\right) \tag{2}$$

Radiative heat transfer coefficient between seawater and the glass cover $h_{r,sw\text{-}gc}$ [32]:

$$h_{r,sw\text{-}gc}=\frac{\sigma\left(T_{sw}+T_{gc}\right)\left(T_{sw}^{2}+T_{gc}^{2}\right)}{1/\varepsilon_{sw}+1/\varepsilon_{gc}-1} \tag{3}$$

σ is Stefan-Boltzmann constant. ε_{sw} is the emissivity of seawater. ε_{gc} is the emissivity of the glass cover.

Convective heat transfer rate between seawater and glass cover $q_{c,sw\text{-}gc}$:

$$q_{c,sw\text{-}gc}=h_{c,sw\text{-}gc}\left(T_{sw}-T_{gc}\right) \tag{4}$$

Convective heat transfer coefficient between seawater and the glass cover $h_{c,sw\text{-}gc}$ [33]:

$$h_{c,sw\text{-}gc} = 0.884 \times \left[T_{sw} - T_{gc} + \frac{\left(p_{sw} - p_{gc}\right)T_{sw}}{268900 - p_{sw}} \right]^{\frac{1}{3}} \tag{5}$$

Water vapor pressure near the sea surface p_{sw} and near the glass cover p_{gc}:

$$p_{sw} = \exp\left(25.317 - \frac{5144}{T_{sw}}\right) \tag{6}$$

$$p_{gc} = \exp\left(25.317 - \frac{5144}{T_{gc}}\right) \tag{7}$$

Evaporative heat transfer rate between seawater surface and glass cover $q_{e,sw}$:

$$q_{e,sw} = h_{e,sw-gc}\left(T_{sw} - T_{gc}\right) \tag{8}$$

Evaporative heat transfer coefficient between the seawater surface and glass cover $h_{e,sw\text{-}gc}$ [33]:

$$h_{e,sw\text{-}gc} = 16.273 \times 10^{-3} h_{c,sw-gc}(p_{sw} - p_{gc}) / (T_{sw} - T_{gc}) \tag{9}$$

Radiative heat transfer rate between the glass cover and the sky $q_{r,gc\text{-}s}$:

$$q_{r,gc-s} = h_{r,gc-s}(T_{gc} - T_s) \tag{10}$$

Radiative heat transfer coefficient between the glass cover and the sky $h_{r,gc-s}$ [33]:

$$h_{r,gc-s} = \varepsilon_{gc}\sigma(T_{gc}^2 + T_s^2)(T_{gc} + T_s) \tag{11}$$

Sky temperature T_s is calculated from ambient temperature T_a, K:

$$T_s = 0.0552 \times T_a^{1.5} \tag{12}$$

Convective heat transfer rate between glass cover and external environment $q_{c,gc\text{-}a}$:

$$q_{c,gc\text{-}a} = h_{c,gc\text{-}a}\left(T_{gc} - T_a\right) \tag{13}$$

Convective heat transfer coefficient between glass cover and external environment $h_{c,gc\text{-}a}$ [34]:

$$h_{c,gc\text{-}a} = 2.8 + 3v_{wind} \tag{14}$$

v_{wind} is the ambient wind speed.

(2) The heat balance equation of the seawater layer is:

$$\alpha_{sw}\tau_{gc}G + q_{c,hss\text{-}sw} = q_{r,sw\text{-}gc} + q_{c,sw\text{-}gc} + q_{e,sw} + C_{p,sw}M_{sw}\frac{\mathrm{d}T_{sw}}{\mathrm{d}\tau} \tag{15}$$

Convective heat transfer rate between seawater and the heat storage surface

$q_{c,hss\text{-}sw}$:

$$q_{c,hss\text{-}sw} = h_{c,hss\text{-}sw}\left(T_{hss} - T_{sw}\right) \tag{16}$$

Convective heat transfer coefficient between seawater and the heat storage surface $h_{c,hss\text{-}sw}$ is selected from [35], $h_{c,hss\text{-}sw}$ =475 W/(m^2·K).

(3) The heat balance equation of the heat storage surface is:

$$\alpha_{hss}\tau_{gc}\left(1-\alpha_{sw}\right)G = q_{c,hss\text{-}sw} + q_{h,hss\text{-}hs} + C_{p,hss}M_{hss}\frac{\mathrm{d}T_{hss}}{\mathrm{d}\tau} \tag{17}$$

It is assumed that the surface layer is the top layer of the rock layer. The solar radiation through the seawater layer is mainly absorbed by the heat storage surface, and then the heat is transferred down to the rock heat storage layer, which is similar to the heat transfer in the solar air heater in the absorption plate and the rock heat storage [36].

Thermal conductivity of the surface layer of the heat storage to the heat storage layer $q_{h,hss\text{-}hs}$:

$$q_{h,hss\text{-}hs} = \frac{\lambda_{hs}}{\delta_{hs}}\left(T_{hss} - T_b\right) \tag{18}$$

The calculation of the effective thermal conductivity of the rock heat storage layer needs to consider the porosity of the layer, which is the weighted average of the thermal conductivity of liquids and solids in the layer [37], so the effective thermal conductivity of the rock heat storage layer λ_{hs}:

$$\lambda_{hs} = \phi\lambda_f + \left(1-\phi\right)\lambda_s \tag{19}$$

In the above equation, λ_f and λ_s are the thermal conductivity of liquid seawater and solid rocks in the layer, W/(m·K), respectively. ϕ is the porosity of the layer, determined by the way the rock particles are accumulated. Here, the rock shape is assumed to be approximately equal-diameter sphere arranged in a body-centered cubic stacking mode, as shown in Fig. 13. The corresponding equation for ϕ is:

$$\phi = 1 - \left(2\cdot\frac{4}{3}\pi r^3\right)\Big/\left(\frac{4}{\sqrt{3}}r\right)^3 = 32\% \tag{20}$$

The effective specific heat capacity $C_{p,hss}$ and mass per unit area M_{hss} of the surface layer:

$$C_{p,hss} = \phi C_{p,f} + \left(1-\phi\right)C_{p,s} \tag{21}$$

$$M_{hss} = \left(\phi\rho_f + \left(1-\phi\right)\rho_s\right)d_p \tag{22}$$

where, $C_{p,f}$ and $C_{p,s}$ are the specific heat capacities of liquid seawater and solid rocks in the surface layer, J/(kg·K), respectively. ρ_f and ρ_s are the densities of liquid seawater and solid rocks in the surface layer, kg/m^3, respectively. d_p is the average particle diameter of the rocks, m.

(4) The heat balance equation of the bottom plate is:

$$q_{h,hs\text{-}b} = q_{h,b\text{-}a} + C_{p,b} M_b \frac{\mathrm{d}T_b}{\mathrm{d}\tau} \tag{23}$$

Since the rock heat storage layer is laid on the bottom plate of the still, the contact thermal resistance between the heat storage layer and the bottom plate is small and negligible, so $q_{h,hs\text{-}b} = q_{h,hss\text{-}hs}$.

Thermal conductivity of the bottom plate to the insulation layer $q_{h,b\text{-}a}$:

$$q_{h,b\text{-}a} = \frac{\lambda_{ins}}{\delta_{ins}}\left(T_b - T_a\right) \tag{24}$$

λ_{ins} is the thermal conductivity of the insulation layer, W/(m·K). δ_{ins} is the thickness of the insulation layer, m.

The hourly water production of the still M_{disc}:

$$M_{disc} = \sum_{i=1}^{60/\Delta t} \frac{q_{e,sw,i}}{h_{fg,sw,i}} A_{disc} \times 60\Delta t \tag{25}$$

where, i is the time node; Δt is the time step, 5 min; A_{disc} is the horizontal evaporation area of the still, m^2.

The initial conditions are: $t = 0$; $\tau = m$, $T = T_a(\tau)$ K

Meteorological conditions are based on a meteorological function model [31]:

$$T_a = 273.15 + \overline{t_{avg}} + \Delta t \cos\left(\frac{\pi}{12}(\tau - 14)\right) \tag{26}$$

$$G = G_{\max} \sin\left(\frac{\tau - m}{n - m}\pi\right), \quad m < \tau < n \tag{27}$$

where, $\overline{t_{avg}}$ and Δt indicate the daily average value and daily variation value of ambient temperature respectively. $G_{\max}$ is the maximum daily solar irradiance. m and n indicate the time of sunrise and sunset, respectively.

4.2 Model validation

In order to verify the correctness and rationality of the mathematical model of the rock enhanced SS, the structural parameters of the still used for the simulation were adopted from the basic structural dimensions of the test setup. Since the shape of the rock is approximated as an equal-diameter sphere, the particle size of the equal-diameter sphere, which is close to the volume of the gray pebbles used in the test, is 2.5

cm. Also, since the spheres are arranged in a body-centered cubic stacking mode, the porosity is 32%. The climatic conditions measured on the test day of September 8, 2021, as described above, are taken for the simulations: $\bar{t}_{avg} = 25.2$ °C, $\Delta t = 3.4$ °C, $G_{max} = 800$ W/m^2, $m = 5{:}50$, $n = 18{:}20$. The mathematical model was programmed with Matlab in a time step of 5 minutes. The numerical calculation process is shown in Fig. 14, which can calculate the temperature distribution and freshwater output during the all-weather operation of the rock enhanced SS.

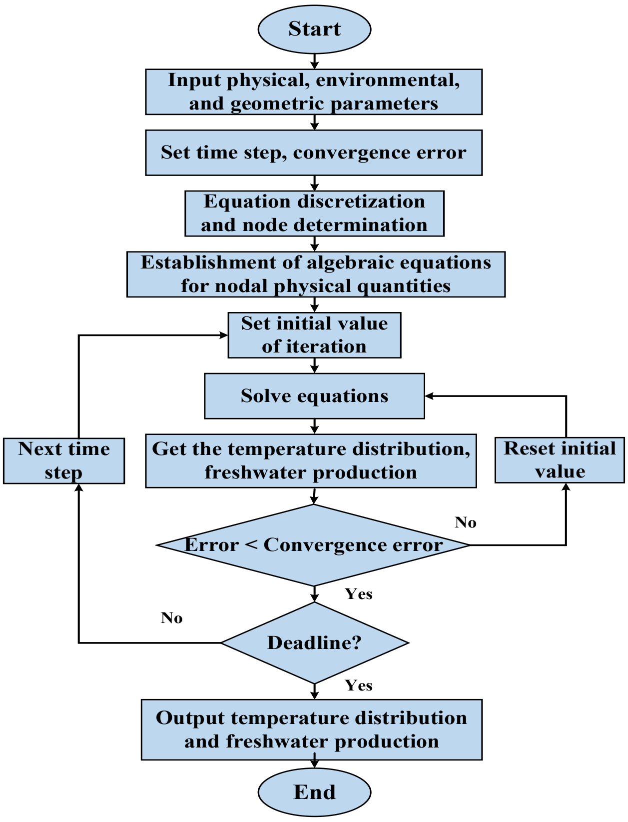

Fig.14. Flow chart of numerical solution

The reasonableness and reliability of the numerical results need to be compared with the test results, and the validity of the comparison is expressed by the correlation coefficient r, and the proximity to the test results can be expressed by the root mean square e. The correlation coefficient r and root mean square e are modeled as [38]:

$$r = \frac{N\sum x_i y_i - \sum(x_i)\sum(y_i)}{\sqrt{N\sum x_i^2 - (\sum x_i)^2}\sqrt{N\sum y_i^2 - (\sum y_i)^2}} \tag{28}$$

where, N is the number of variables; x_i and y_i are the calculated and experimental value, respectively. $0.8 \le |r| < 1$ indicates a high correlation; $0.5 \le |r| < 0.8$ indicates a significant correlation; $0.3 \le |r| < 0.5$ indicates a low correlation; $0 < |r| < 0.3$ indicates a weak correlation.

$$e = \sqrt{\frac{\sum (e_i)^2}{N}} \tag{29}$$

where, $e_i = \dfrac{x_i - y_i}{x_i}$.

If the r value is in the high correlation region; e is less than 5% and can exceed 5% for special reasons, it means that the model calculated value and the test value are in better agreement, and the model simulation effect is acceptable.

Fig. 15 shows the curves of the experimental values compared to the calculated values for the operation of the rock enhanced SS. Table 3 is a statistical summary table comparing the experimental and calculated values.

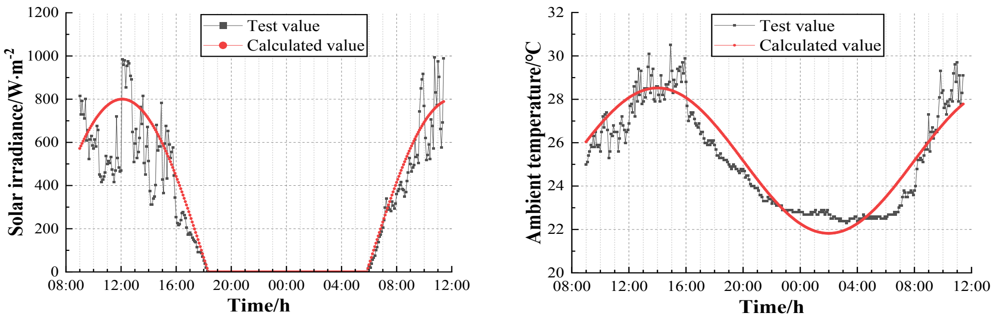

(a) Solar irradiance **(b) Ambient temperature**

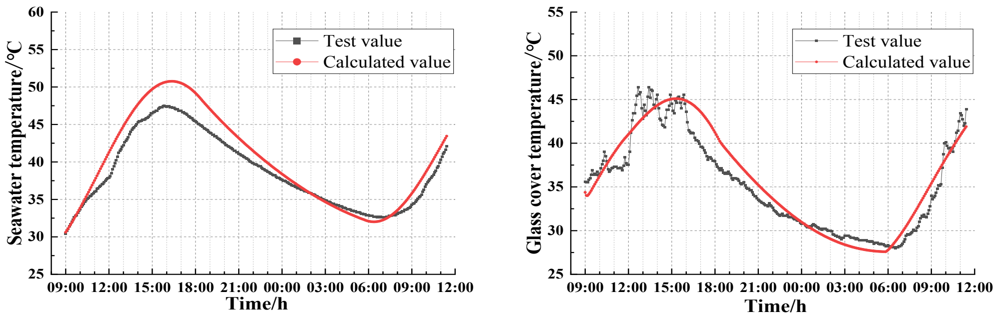

(c) Seawater temperature **(d) Glass cover temperature**

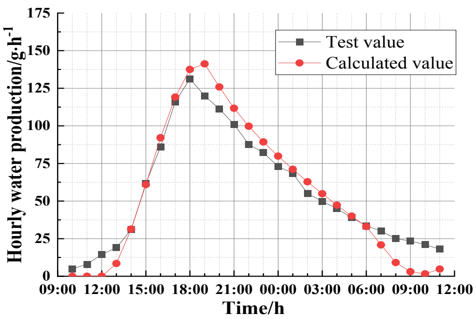

(e) Hourly water production

Fig.15. Comparison curves of experimental and calculated values

Table 3 Statistical summary table comparing the experimental and calculated values

Statistical analysis	*r*%	*e*%
Solar irradiance	93.51	20.44
Ambient temperature	93.67	3.26
Seawater temperature	99.44	4.47
Glass cover temperature	95.56	4.68
Hourly water production	99.09	31.02

As can be seen from Fig. 15 and Table 3, the calculated values are in good agreement with the experimental values, and can better reflect the experimental values. Among them, the root mean square deviation of solar irradiance is mainly caused by the large number of mutant singularities measured during the period when the solar irradiation level is high at noon. The root mean square deviation of the water production of the still is large, which is reflected in the fact that the calculated value of the water production from 9:00 to 12:00 is zero, which is low, and the calculated value of the water production in other periods is higher than the experimental value. The main reason is that when the temperature difference between seawater and cover is negative, it is assumed that the entire still does not produce freshwater and the freshwater output is zero. However, when the temperature difference between the seawater and the cover plate at the measuring point in the center of the cover plate is negative, the temperature difference at other locations of the cover plate is not negative at the same time, and there will still be water vapor condensation at these locations to produce a certain amount of freshwater. Therefore, the calculated values for this period are lower than the experimental values. In other periods, the calculated value of water produced is higher than the test value. It is because some of the distilled water condensed on the inside of the glass cover drips back to the still on the way to the collection slot and is not collected, which makes the test water volume small, and the heat loss caused by the poor sealing of the still will also make the test water volume small.

5. Analysis of the impact of core parameters of rock enhanced solar still

In order to further improve the daily water production and energy utilization efficiency of the rock enhanced SS, optimizing the parameter configuration of the rock heat storage layer is a feasible approach. Therefore, it is necessary to explore the operation and output of the rock enhanced SS under different heat storage layer thicknesses, rock particle sizes and rock materials under the designed environmental conditions based on the established mathematical model. The design environmental conditions are: $\bar{t}_{\text{avg}} = 28$ °C, $\Delta t = 4$ °C, $G_{\max} = 1000$ W/m^2, $m = $ 6:00, $n = $ 18:00, $v_{wind} = 1.5$ m/s. The basic structural design parameters of the rock enhanced SS in the analysis are the same as those of the test device, and the seawater depth is $H_w = 0.1$ m. Among them, the rock material in the still is pebble, with an average particle size $d_p = 2.5$ cm. The rock heat storage layer is composed of two layers of pebbles arranged in a body-centered cubic stacking mode, and the thickness of the heat storage layer is $H_{sm} = 0.0394$ m, and the porosity of the rock heat storage layer is $\phi = 32$ %.

5.1 Effect of rock heat storage layer thickness

The pebbles in the still have an average particle size $d_p = 2.5$ cm and are arranged in a body-centered cubic stacking mode to form a rock heat storage layer. When the seawater level is 10 cm, the correspondence between the number of rock heat storage layers and the thickness of rock heat storage layer and seawater layer is shown in Table 4.

Table 4 Correspondence between the number of layers and thickness of the rock heat storage layer

Number of heat storage layers	One	Two	Three	Four	Five
Thickness of heat storage layer/cm	2.50	3.94	5.39	6.83	8.27
Thickness of seawater layer/cm	7.50	6.06	4.61	3.17	1.73

Fig. 16, 17, 18 and 19 show the variation curves of hourly water production, seawater temperature, seawater-cover temperature difference and heat exchange rate per unit area between the heat storage layer and seawater under the same seawater level and different heat storage layer thicknesses, respectively.

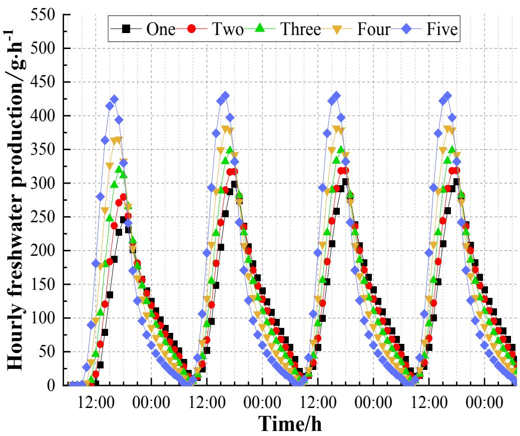

Fig. 16. Hourly water production

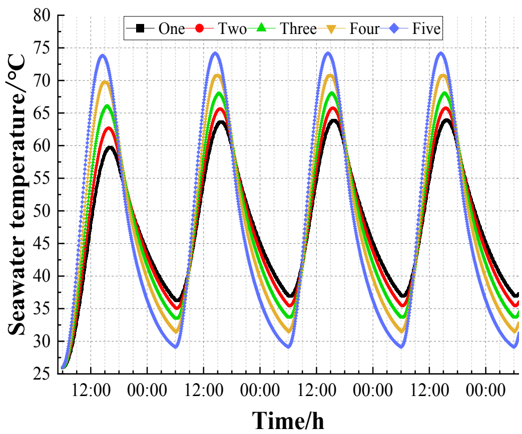

Fig. 17. Seawater temperature

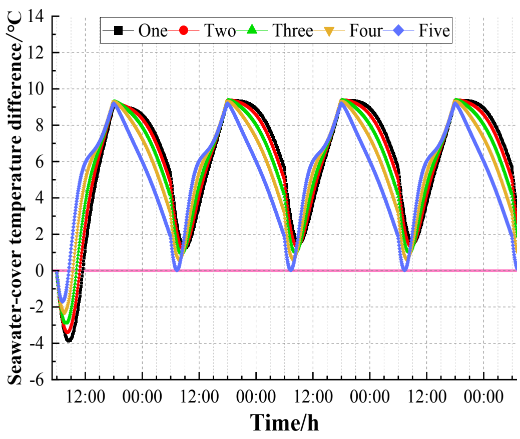

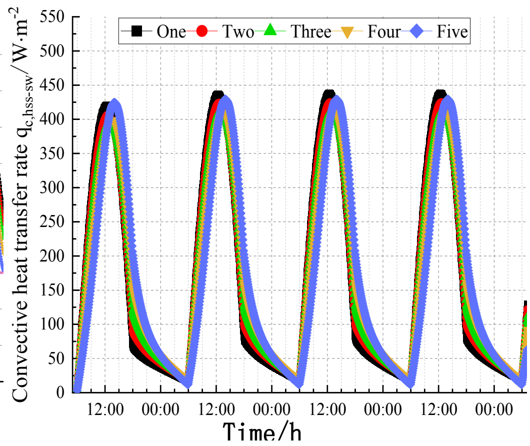

Fig. 18. Seawater-cover temperature difference Fig. 19. Convective heat transfer rate

As can be seen from Fig. 16, on the fourth day of stable operation, with the increase in the number of rock heat storage layers from one to five, the water production and the peak value in the rising period increased more, and the peak point shifted to the left more significantly. The water production and troughs decreased during the period of declining water production, but the decrease in troughs was not significant and the leftward shift of the trough point was also not significant, and the daily fluctuations in water production increased. This is mainly due to the fact that with the increase of the rock layer, the thickness of seawater decreases, the heat capacity of seawater decreases, the thermal inertia decreases, and the seawater temperature and seawater-cover temperature difference are more likely to rise and fall. That is, after sunrise, the temperature of the seawater with a smaller thickness rises earlier, faster and higher (Fig. 17). The same is true of the seawater-cover temperature difference (Fig. 18), so the peak point of water production is shifted to the left, and the peak value is higher. After the peak, both seawater temperature and seawater-cover temperature difference drop faster and lower with smaller seawater thickness. Although the heat released from the heat storage layer to seawater at night increases with the increase of the thickness of the rock heat storage layer (Fig. 19), the heat released does not change the trend of seawater temperature decline due to the existence of heat dissipation loss, but only slows down the seawater temperature decline rate and magnitude, so the decrease of the trough point of water production and the left shift are not significant.

Fig. 20 is a histogram comparing the total daily, daytime and night water production of the still during stable operation on the fourth day under the same seawater level and different heat storage layer thicknesses. The daytime water production period is 6:00-18:00, and the night water production period is 18:00-6:00. It can be seen from the figure that with the increase of the thickness of the heat storage layer, the total daily water production shows a gradual upward trend. The water production of the still was dominated by nighttime water production (53.87% of the total water production under the condition of one layer of heat storage layer) and gradually changed to be dominated by daytime water production (73.59% of the total water production under the condition of five layers of heat storage layer), and the difference between day and night water production gradually increased. This is because a thicker heat storage layer at the same seawater level leads to a reduction in seawater volume, a faster warming of seawater during sunshine, and a higher overall seawater temperature. This leads to an increase in the positive temperature difference between the seawater and the glass cover, which is very favorable to the water production in the peak production region [31]. The increase in daytime water production compensated for the dip in nighttime water production caused by the decrease in the thermal storage capacity of the SS, thus increasing the total water production.

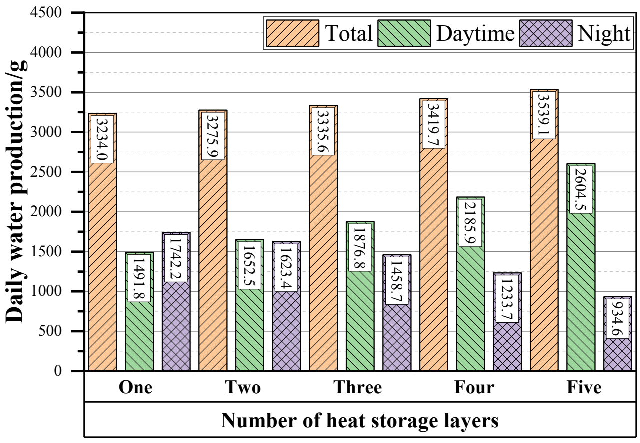

Fig.20. Daily water production with different heat storage thicknesses

Fig. 21 and Fig. 22 show the variation curve of the daily and cumulative water production of the rock enhanced SS under different heat storage layer thicknesses. As can be seen from Fig. 21, as the thickness of the heat storage layer increases and the thickness of the seawater layer decreases, the number of days required for the device to enter stable operation gradually decreases, and the stable water production begins earlier. This is because the reduction of seawater shortens the process of seawater heat absorption and heat storage at the beginning of the operation of the device, and when the thickness of the heat storage layer is 8.27 cm and the thickness of the seawater layer is 1.73 cm (corresponding to the five layers), the still basically reaches stable operation on the second day of operation. It can be seen from Fig. 22 that when the heat storage layer is thicker and the seawater layer is thinner, the period when the curve slope changes significantly shortens but the magnitude of the slope change increases, and the period when the curve slope tends to zero is prolonged. It indicates that with the increase of the thickness of the heat storage layer, the peak water production period of SS is shortened, but the peak water production volume rises, the trough water production period is prolonged, the fluctuation of the cumulative water production curve becomes more and more violent, and the equilibrium and continuity of the water production are destroyed. However, the total cumulative water production is significantly increased.

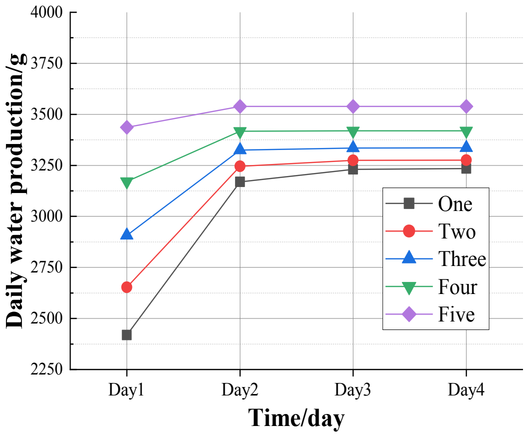

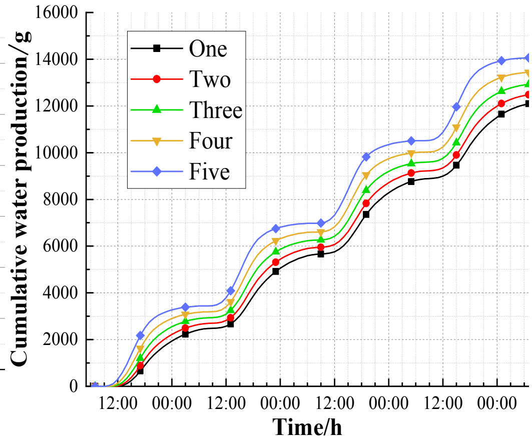

Fig.21. Variation curve of daily water production Fig.22. Variation curve of cumulative water production

From the perspective of increasing water production, the water production of the still under the five-layer heat storage layer has obviously been improved. However, the increase of the thickness of the heat storage layer and the decrease of seawater volume will worsen the balance of the hourly water production distribution of the still and the balance of diurnal water production, which is not conducive to the stable water production of the still. Therefore, as a compromise, the thickness of the 5.39 cm heat storage layer corresponding to the three-layer layer with a particle size of 2.5 cm was taken for follow-up research.

5.2 Effect of rock particle size

It is necessary to explore the effect of rock particle size on the operation and output performance of the still at a thickness of 5.39 cm. Since the rocks are arranged in a body-centered cubic stacking mode, there is a correspondence between the rock particle size and the number of layers shown in Table 5 when the thickness of the heat storage layer is guaranteed at 5.39 cm.

Table 5 Correspondence between rock particle size and the number of layers

Number of heat storage layers	2	3	4	5	6
Rock particle size/cm	3.42	2.50	1.97	1.63	1.39

Fig. 23 shows the variation curves of hourly water production under different rock particle sizes. Fig. 24 shows the temperature curve of the heat storage surface layer. Fig. 25 shows the variation curve of convective heat transfer rate per unit area between the surface layer of heat storage and seawater. Fig. 26 shows the curve of seawater temperature. Fig. 27 shows the seawater-cover temperature difference.

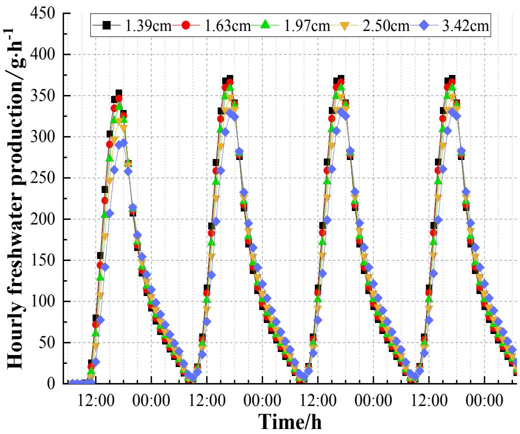

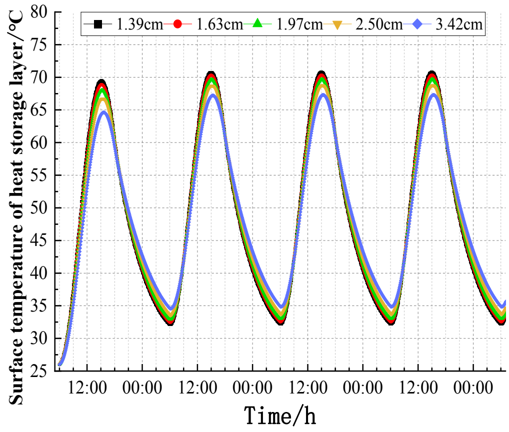

Fig. 23. Hourly water production **Fig. 24. Surface temperature of heat storage layer**

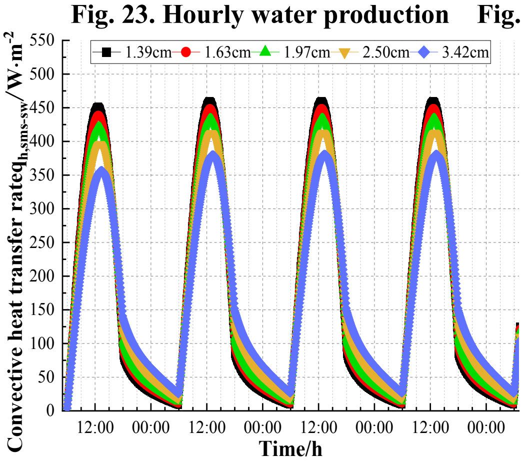

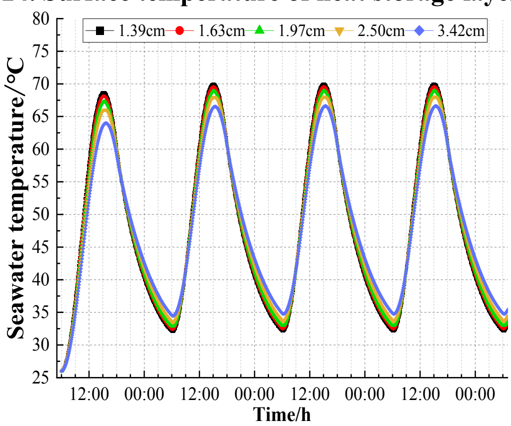

Fig. 25. Convective heat transfer rate **Fig. 26. Seawater temperature**

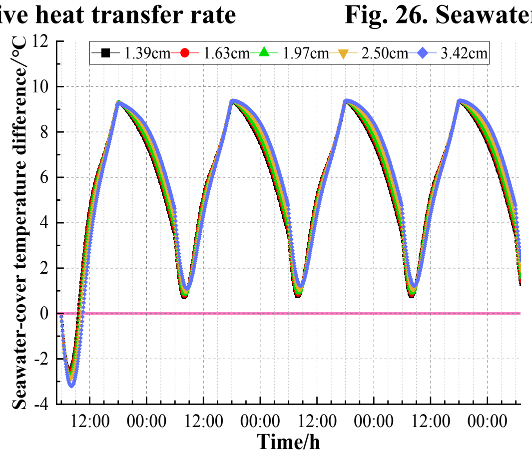

Fig. 27. Seawater-cover temperature difference

It can be seen from Fig. 23 that on the fourth day of stable operation, with the increase of rock particle size, from 1.39 cm to 3.42 cm, the peak point of hourly water production in the still decreases greater, and the peak point shifts to the right; the valley value increases slightly, the valley point moves slightly to the right, and the daily fluctuation of water production decreases. This is due to the increase in particle size, the thickness of the heat storage surface layer increases, the amount of heat storage increases, and the heat capacity and thermal inertia increase. Under the same solar radiation, the larger the particle size, the slower the heating rate of the rock heat storage surface layer, the lower the rise, and the greater the decrease in the temperature rise, the more the peak point shifts to the right (Fig.24), which in turn affects the degree of decline of the convective heat transfer rate per unit area between the heat storage surface layer and the seawater, making the more decrease (Fig. 25). As a result, the seawater temperature rise was the lowest, the peak seawater temperature shifted to the right the most (Fig. 26), and the seawater-cover temperature difference was also the lowest (Fig. 27). Therefore, the increase in water production during this period was relatively low, and the peak point shifted to the right. In the absence of solar radiation, the larger the particle size, the larger the heat storage stores more heat, and the temperature drop of the heat storage itself slows down, which is better able to release heat to the seawater (Fig. 25), slows down the cooling rate of the seawater (Fig. 26), and maintains a high seawater-cover temperature difference (Fig. 27). Therefore, the decline of water production was relatively slowest during this period, and the trough value of water production increased slightly. This phenomenon indicates that for rock heat storage, increasing the particle size appropriately is conducive to improving the uneven distribution of daily water production.

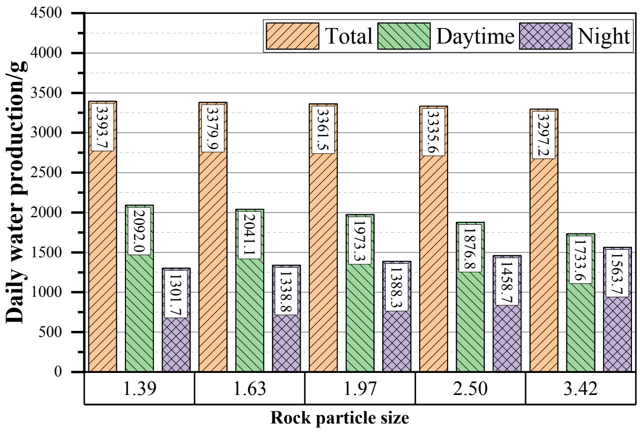

Fig. 28. Daily water production

Fig. 28 shows the histogram of the total daily, daytime and night water production of the still on the fourth day under different rock particle sizes. It can be seen from the figure that with the increase of rock particle size, the daily water production shows a gradual decrease trend. In this case, water production decreased during the day and increased at night. This is because the increase in rock particle size increases the amount of heat stored in the rock heat storage surface layer, leading to a decrease in its overall temperature during sunlight, which in turn affects the temperature of the seawater, that relies on the absorption of its heat transfer for warming, as well as the seawater-cover temperature difference, resulting in a natural decrease in the amount of water produced during the daytime. At night, the water production increased slightly due to the increased heat stored in the heat storage layer as a result of the increased particle size, which maintained the temperature of the whole system at a higher level. As the decrease in daytime water production was slightly higher than the increase in nighttime water production, the daily water production declined slightly, but the difference in daytime and nighttime water production decreased significantly, from 790.3 g at 1.39 cm to 169.9 g at 3.42 cm. The above analysis indicates that the rock particle size has a limited effect on the total water production, but has an effect on the equalization of the daily distribution of water production in the still. The larger the particle size, the more equalized the distribution of water production during day and night.

Fig. 29 and Fig. 30 show the variation curve of the daily and cumulative water production of the rock enhanced SS under different rock particle sizes. As can be seen from Fig. 29, under the same thickness of the heat storage layer and different particle sizes, the device basically enters stable operation after 2-3 days of operation. It shows that the size of the rock particle size has an effect on the number of days or time required for the device to enter stable operation, but it is not significant. At the beginning of operation, especially on the first day, the difference of daily water production under different particle sizes is larger, and the smaller the particle size, the higher the daily water production. With the increase of operation days, the difference in daily water production under different particle sizes becomes smaller and smaller until stabilized. It can also be seen from Fig. 30 that after the device is stabilized, the larger the rock particle size is, the more gentle the fluctuation of the cumulative water production curve is, and the more balanced the distribution of water production is. The cumulative total water production has decreased.

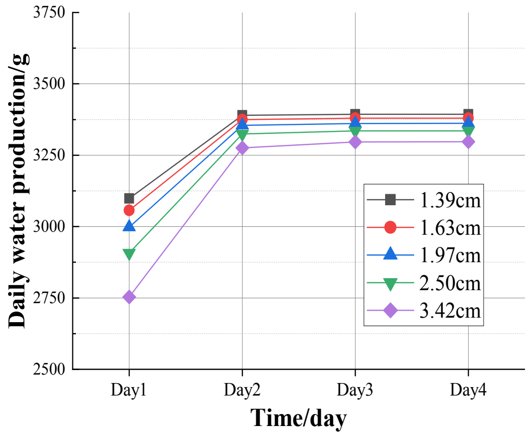

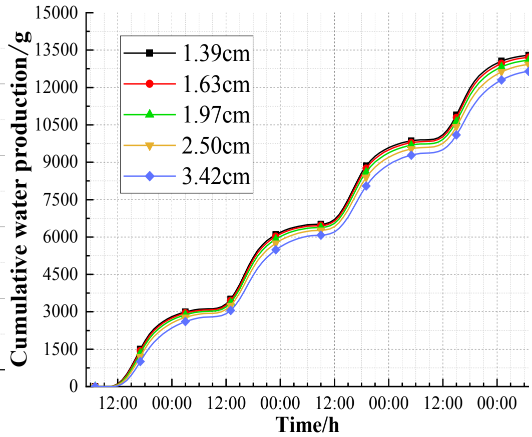

Fig.29. Variation curve of daily water production Fig.30. Variation curve of cumulative water production

Because the influence of rock particle size on the total water production is limited, it mainly affects the average distribution of daily water production of the still. The larger the particle size, the more balanced the distribution of water production day and night. However, the particle size is too large, it is not easy to control the desired thickness of the heat storage layer. Therefore, it is considered that the current design of rock particle size is more reasonable. In the following study, the rock particle size of 2.5 cm is still used.

5.3 Effect of rock material

Table 6 summarizes the physical parameters of the five common rock materials selected, ranked in order of heat capacity.

Table 6 Table of physical parameters of selected rock materials

Rock material	Density /kg·m^{-3}	Specific heat capacity /J·kg^{-1}· K^{-1}	Heat capacity /KJ·m^{-3}· K^{-1}	Thermal conductivity /W·m^{-1}· K^{-1}
Red brick	1800	840	1512.00	0.86
Quartzite	2650	775	2053.75	6.18
Pebble	2563	820	2101.66	2.07
Metal stone	2323	980	2276.54	1.83
Basalt	2900	1230	3567.00	1.69

Fig. 31 shows the variation curve of hourly water production under different rock materials. Fig. 32 shows the temperature curve of the heat storage surface layer. Fig. 33 shows the variation curve of convective heat transfer rate per unit area between the surface layer of heat storage and seawater. Fig. 34 shows the curve of seawater temperature. Fig. 35 shows the seawater-cover temperature difference.

It can be seen from Fig. 31 that on the fourth day of stable operation, when the rock material is red brick, the peak hourly water production is the highest, the trough value is the lowest, and the daily fluctuation range of water production is the largest. When the rock material is basalt, the peak hourly water production is the lowest, the trough value is relatively highest, and the daily fluctuation range of water production is the smallest. The hourly water production of other heat storage materials varies between the two, and the difference in their water production is small. This is because the amount of heat stored in the rock heat storage depends mainly on the heat capacity of the rock material. The higher the heat capacity, the more heat it stores and the greater the thermal inertness. For the same solar irradiance, the surface layer of a material's heat storage heats up with a lag, the slower it heats up, and the lower it heats up. When there is no solar irradiation, the temperature drop in the heat storage layer itself is slowed down as the rock with the higher heat capacity stores more heat. Therefore, the use of the larger heat capacity of the rock as a heat storage layer, the stills exhibit similar operating characteristics and mechanisms as those exhibited by the larger particle size of the heat storage layer, as can also be seen from the corresponding comparison of Fig. 32-Fig. 35 with the previous Fig. 24-Fig. 27. Red brick has the smallest heat capacity, and basalt has the largest heat capacity. Because the heat capacity of quartzite, pebble, and metal stone is similar, between that of red brick and basalt, their hourly water production varies between that of red brick and basalt, and the difference is small.

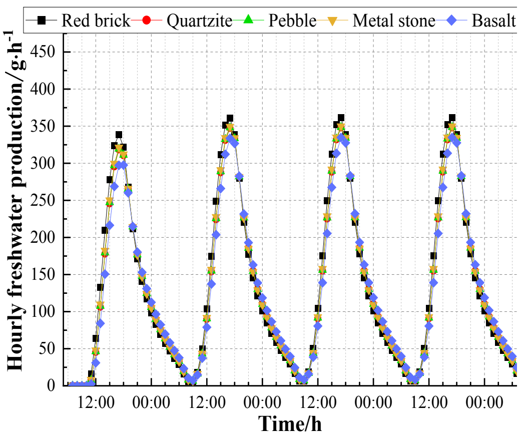

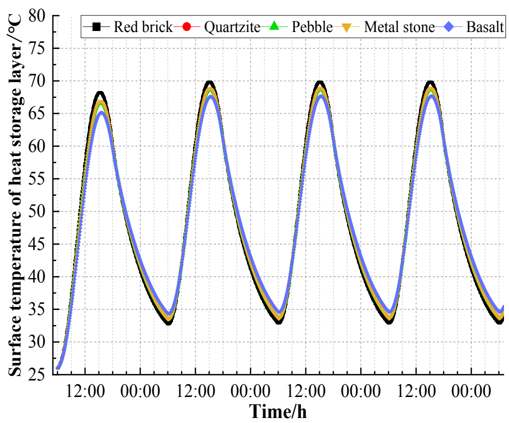

Fig. 31. Hourly water production **Fig. 32. Surface temperature of heat storage layer**

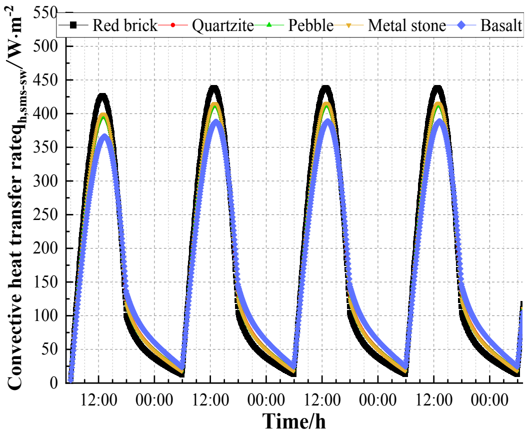

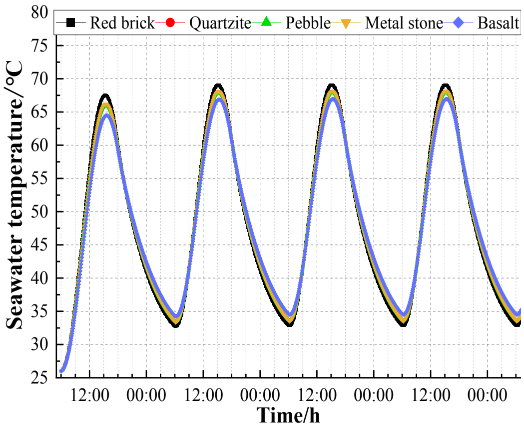

Fig. 33. Convective heat transfer rate **Fig. 34. Seawater temperature**

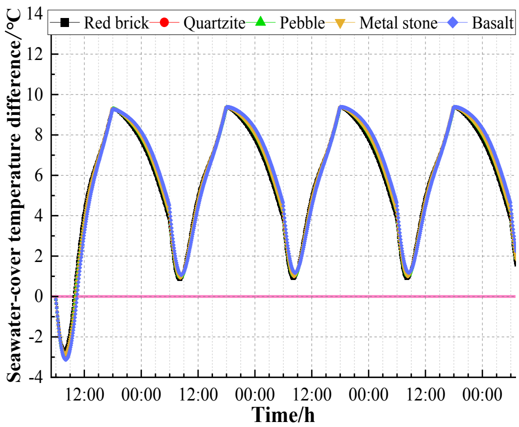

Fig. 35. Seawater-cover temperature difference

Fig. 36 shows the histogram of the total daily, daytime and night water production of the still on the fourth day under different rock materials. It can be seen from the figure that the daily water production of rock materials from red brick to basalt gradually decreases with the increase of the heat capacity of the materials, but the decrease is limited. Among them, the daytime water production decreased, the night water production increased, and the still significantly reduced the difference between day and night water production, from the red brick when the difference of 615.9 g to basalt when the difference of 226.6 g. This indicates that the common rock materials have limited influence on the total water production, but have some influence on the daily water production of the still.

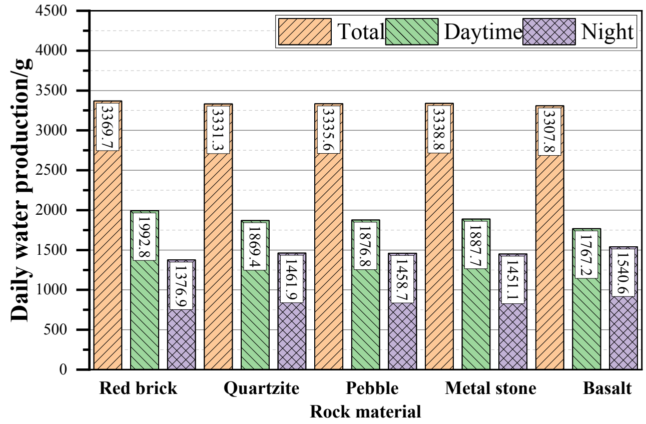

Fig.36. Daily water production

Fig. 37 and Fig. 38 shows the variation curve of the daily and cumulative water production of the still under different rock materials. As can be seen from Fig. 37, there are some differences in the number of days or times for the device to enter stable operation under different rock materials, indicating that the rock materials have some influence on the time required for the stable operation of the device. On the first day of operation, the difference of daily water production under different materials was slightly larger, and the daily water production of red brick with the smallest heat capacity was relatively high. As the number of days or hours of operation increases, the difference in daily water production under different materials becomes smaller and smaller until it is stable. It can also be seen from Fig. 38 that after stable operation of the device, the larger the heat capacity, the more gentle the fluctuation of the cumulative water production curve, and the more balanced the distribution of water production. The cumulative total water production has decreased.

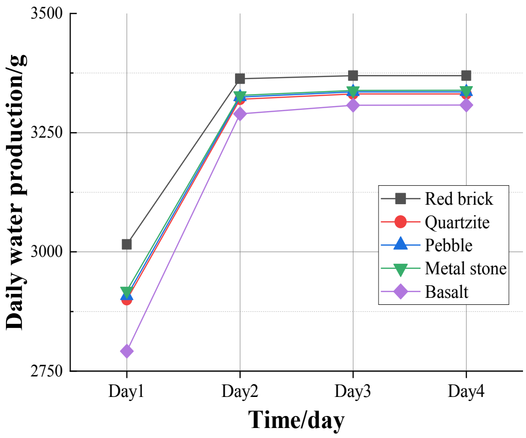

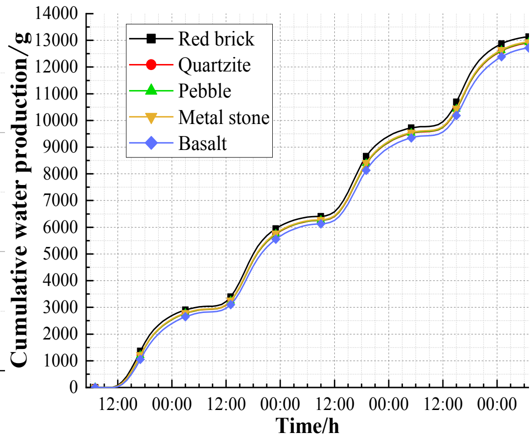

Fig.37. Variation curve of daily water production Fig.38. Variation curve of cumulative water production

In short, when selecting rock materials, in addition to considering the influence of rock materials on the balance of daily water production, the rationality of the price of rock materials can be comprehensively considered. Among the above five materials, red brick and pebble are relatively cheap [33] and red bricks are used as rock materials due to their higher daily water production.

According to the theoretical analysis of the influence of the design parameters, the design parameters of the rock enhanced SS were optimally, and the basic design parameters were as follows: the thickness of the heat storage layer was 5.39 cm, the rock particle size was 2.5 cm, and the rock material was red brick. The daily water production of the rock enhanced SS was 3369.7 g, which was 2.86% higher than that before the optimal configuration, and 4.84% higher than that of the traditional basin SS.

6. Conclusion

In this paper, the test platforms of membrane distillation, rock, corrugated plate enhanced SSs and traditional SS were designed and built. And under the actual meteorological conditions, the operation rules and output characteristics of four SSs were compared horizontally through experiments to explore the effects of the three enhanced measures. An unsteady physical and mathematical model of the rock enhanced SS was established, and the model was verified based on the experimental data, and the effects of rock heat storage layer thickness, rock particle size and rock material on the performance of the rock enhanced SS were investigated. The conclusions are as follows:

(1) The use of the above three enhanced measures in the traditional still will affect the magnitude of changes in seawater and cover temperature, but not the change trend. The laying of rocks or corrugated plate can mainly increase the seawater temperature and the seawater-cover temperature difference in the rising and peak areas of the produced water, and enhance the distillation and heat storage effects of the still, in which the enhanced effect of the corrugated plate is relatively better. The coupled membrane distillation will increase the heat loss from the seawater, resulting in a lower seawater temperature and seawater-cover temperature difference than in a traditional still, which explains the importance of recycling the latent heat of condensation released from condensation of water vapor on condensation plate back into the still.

(2) All three enhanced measures can increase the water production of the still, and the increase of water production is mainly concentrated in the rising and peak areas of water production, and the difference of water production of each still in the decreasing period is relatively small. The peak water production of the four stills is the same, all

around 18:00. During the test period, the total water production of rock, corrugated plate and membrane distillation enhanced SS were 1456.1 g, 1537.1 g and 1528.0 g, respectively, which were 6.38%, 12.30% and 11.63% higher than those of traditional SS.

(3) The calculation results of the unsteady physical mathematical model of the rock enhanced SS constructed based on the body-centered cubic stacking mode technology are in good agreement with the experimental data, which can effectively predict the operation and output characteristics of the still under the rock enhanced technology in a specific environment.

(4) Under the same water level, the increase of the thickness of the rock heat storage layer, the decrease of the rock particle size and the heat capacity of the rock material will increase the water production in the rising and peak areas of the still, reduce the water production in the falling period, and increase the total daily water production. Among them, the influence of rock particle size and rock material on the total daily water production is weak, and the increase of the thickness of the heat storage layer will aggravate the fluctuation of water production, although the increase of water production is more obvious. The selection of the above parameters should take into account the effect of water production enhancement and water production balance, and the selection of rock materials should also consider the price cost. The optimized configuration was a heat storage layer with a thickness of 5.39 cm, a rock particle size of 2.5 cm and a rock material of red brick. The optimized daily water production was 3369.7 g, which was 2.86% higher than the pre-optimization one and 4.84% higher than that of the conventional SS.

Future studies will take into account the change in values after extending the number of test cycles, as well as water quality analysis of seawater and distilled water outputs.

Acknowledgment

This research was financially supported by National Natural Science Foundation of China (No. 51976053).

References

[1] H. Hassan, O. Omran Osman, S. abo-Elfadl, Novel dynamic simulation model and detailed performance evaluation of single slope solar still: Impact of side walls material, Solar Energy 244 (2022) 298–314. https://doi.org/10.1016/j.solener.2022.08.026.

[2] F.A. Hammad, M.E. Zayed, E. El-Bialy, K. Irshad, Z. Lu, S.M. Shalaby,

Performance assessment of a novel solar distiller with a fountain-shaped basin design embedded with phase change materials enriched with copper oxide nano-additives: A detailed experimental investigation, Journal of Energy Storage 82 (2024) 110555. https://doi.org/10.1016/j.est.2024.110555.

[3] A. Elsheikh, M. Zayed, A. Aboghazala, F.A. Essa, S. Rehman, O. L. Muskens, A. Kamal, M.A. Elaziz, Innovative solar distillation system with prismatic absorber basin: Experimental analysis and LSTM machine learning modeling coupled with great wall construction algorithm, Process Safety and Environmental Protection 186 (2024) 1120–1133. https://doi.org/10.1016/j.psep.2024.04.063.

[4] G.B. Shirsath, K. Muralidhar, R.G.S. Pala, Variable air gap membrane distillation for hybrid solar desalination, Journal of Environmental Chemical Engineering 8 (2020) 103751. https://doi.org/10.1016/j.jece.2020.103751.

[5] L. Zuo, C. Xiao, Z. Yan, L. Huang, Z. Guo, Y. Ge, Characterization and prediction modeling of membrane distillation enhanced disc solar still, Journal of Cleaner Production 449 (2024) 141742. https://doi.org/10.1016/j.jclepro.2024.141742.

[6] M.S. Guney, Y. Tepe, Classification and assessment of energy storage systems, Renewable and Sustainable Energy Reviews 75 (2017) 1187–1197. https://doi.org/10.1016/j.rser.2016.11.102.

[7] M. Abdelgaied, M.E.H. Attia, A.E. Kabeel, M.E. Zayed, Improving the thermo-economic performance of hemispherical solar distiller using copper oxide nanofluids and phase change materials: Experimental and theoretical investigation, Solar Energy Materials and Solar Cells 238 (2022) 111596. https://doi.org/10.1016/j.solmat.2022.111596.

[8] M. Karthick, S. Joe Patrick Gnanaraj, M. Appadurai, S.B. Jeshurun, Productivity Enhancement of a Single Slope Solar Still with Energy Storage Medium, Materials Today: Proceedings 60 (2022) 889–893. https://doi.org/10.1016/j.matpr.2021.09.548.

[9] Z.S. Abdel-Rehim, A. Lasheen, Improving the performance of solar desalination systems, Renewable Energy 30 (2005) 1955–1971. https://doi.org/10.1016/j.renene.2005.01.008.

[10] A.S. Nafey, M. Abdelkader, A. Abdelmotalip, A.A. Mabrouk, Solar still productivity enhancement, Energy Conversion and Management 42 (2001) 1401–1408. https://doi.org/10.1016/S0196-8904(00)00107-2.

[11] K. Kalidasa Murugavel, S. Sivakumar, J. Riaz Ahamed, Kn.K.S.K. Chockalingam, K. Srithar, Single basin double slope solar still with minimum basin depth and energy

storing materials, Applied Energy 87 (2010) 514–523. https://doi.org/10.1016/j.apenergy.2009.07.023.

[12] S.J.P. Gnanaraj, V. Velmurugan, Experimental investigation on the performance of modified single basin double slope solar stills, International Journal of Ambient Energy 43 (2022) 206–215. https://doi.org/10.1080/01430750.2019.1636861.

[13] M. Sakthivel, S. Shanmugasundaram, Effect of energy storage medium (black granite gravel) on the performance of a solar still, International Journal of Energy Research 32 (2008) 68–82. https://doi.org/10.1002/er.1335.

[14] S. Abdallah, M.M. Abu-Khader, O. Badran, Effect of various absorbing materials on the thermal performance of solar stills, Desalination 242 (2009) 128–137. https://doi.org/10.1016/j.desal.2008.03.036.

[15] T.V. Arjunan, H.S. Aybar, P. Sadagopan, B. Sarat Chandran, S. Neelakrishnan, N. Nedunchezhian, The Effect of Energy Storage Materials on the Performance of a Simple Solar Still, Energy Sources, Part A: Recovery, Utilization, and Environmental Effects 36 (2014) 131–141. https://doi.org/10.1080/15567036.2010.493924.

[16] T. Rajaseenivasan, A.P. Tinnokesh, G.R. Kumar, K. Srithar, Glass basin solar still with integrated preheated water supply – Theoretical and experimental investigation, Desalination 398 (2016) 214–221. https://doi.org/10.1016/j.desal.2016.07.041.

[17] S.J.P. Gnanaraj, V. Velmurugan, An experimental study on the efficacy of modifications in enhancing the performance of single basin double slope solar still, Desalination 467 (2019) 12–28. https://doi.org/10.1016/j.desal.2019.05.015.

[18] B. Madhu, E. Balasubramanian, A.E. Kabeel, S.A. El-Agouz, A. Muthu Manokar, N. Prakashe, R. Sathyamurthy, Experimental investigation on the effect of sensible heat energy storage in an inclined solar still with baffles, Dwt 116 (2018) 49–56. https://doi.org/10.5004/dwt.2018.22474.

[19] A. Bilal, B. Jamil, N.U. Haque, M.A. Ansari, Investigating the effect of pumice stones sensible heat storage on the performance of a solar still, Groundwater for Sustainable Development 9 (2019) 100228. https://doi.org/10.1016/j.gsd.2019.100228.

[20] P. Patel, R. Kumar, Comparative Performance Evaluation of Modified Passive Solar Still Using Sensible Heat Storage Material and Increased Frontal Height, Procedia Technology 23 (2016) 431–438. https://doi.org/10.1016/j.protcy.2016.03.047.

[21] A.E. Kabeel, S.A. El-Agouz, R. Sathyamurthy, T. Arunkumar, Augmenting the productivity of solar still using jute cloth knitted with sand heat energy storage, Desalination 443 (2018) 122–129. https://doi.org/10.1016/j.desal.2018.05.026.

[22] A.E. Kabeel, M. Abdelgaied, A. Eisa, Enhancing the performance of single basin solar still using high thermal conductivity sensible storage materials, Journal of Cleaner Production 183 (2018) 20–25. https://doi.org/10.1016/j.jclepro.2018.02.144.
[23] Z.M. Omara, A.E. Kabeel, The Performance of Different Sand Beds Solar Stills, International Journal of Green Energy 11 (2014). https://doi.org/10.1080/15435075.2013.769881.
[24] D.G. Harris Samuel, P.K. Nagarajan, R. Sathyamurthy, S.A. El-Agouz, E. Kannan, Improving the yield of fresh water in conventional solar still using low cost energy storage material, Energy Conversion and Management 112 (2016) 125–134. https://doi.org/10.1016/j.enconman.2015.12.074.
[25] S. Kumaravel, M. Nagaraj, G. Bharathiraja, Experimental investigation on the performance analysis of blue metal stones and pebble stones as thermal energy storage materials in single slope solar still, Materials Today: Proceedings 77 (2023) 430–435. https://doi.org/10.1016/j.matpr.2022.11.100.
[26] A.R. Prasad, M.E.H. Attia, W. Al-Kouz, A. Afzal, M.M. Athikesavan, R. Sathyamurthy, Energy and exergy efficiency analysis of solar still incorporated with copper plate and phosphate pellets as energy storage material, Environ Sci Pollut Res 28 (2021) 48628–48636. https://doi.org/10.1007/s11356-021-14080-5.
[27] N. Muthu Saravanan, S. Rajakumar, A.A.M. Moshi, Experimental investigation on the performance enhancement of single basin double slope solar still using kanchey marbles as sensible heat storage materials, Materials Today: Proceedings 39 (2021) 1600–1604. https://doi.org/10.1016/j.matpr.2020.05.710.
[28] P. Dumka, A. Sharma, Y. Kushwah, A.S. Raghav, D.R. Mishra, Performance evaluation of single slope solar still augmented with sand-filled cotton bags, Journal of Energy Storage 25 (2019) 100888. https://doi.org/10.1016/j.est.2019.100888.
[29] A.F. Mohamed, A.A. Hegazi, G.I. Sultan, E.M.S. El-Said, Enhancement of a solar still performance by inclusion the basalt stones as a porous sensible absorber: Experimental study and thermo-economic analysis, Solar Energy Materials and Solar Cells 200 (2019) 109958. https://doi.org/10.1016/j.solmat.2019.109958.
[30] M.E.H. Attia, A.E. Kabeel, M.E. Zayed, M. Arıcı, M. Abdelgaied, Optimal size of spherical rock salt balls as low-cost thermal storage materials for performance augmentation of hemispherical solar distillers: Experimental investigation and thermo-economic analysis, Journal of Cleaner Production 374 (2022) 134006. https://doi.org/10.1016/j.jclepro.2022.134006.

[31] L. Zuo, Z. Yan, P. Dai, T. Zhou, B. Qu, Y. Yuan, Y. Ge, Experimental research on the operation characteristics of solar chimney power plant combined with distillation (SCPPCD), Applied Energy 326 (2022) 120029. https://doi.org/10.1016/j.apenergy.2022.120029.
[32] ZUO Lu, ZHENG Yuan, SHA Yujun, LI Zhenjie, LIU Wenming, Study on unsteady heat transfer in solar chimney power generation system combined with seawater desalination, Proceedings of the CSEE. 30 (2010) 108–114. https://doi.org/10.13334/j.0258-8013.pcsee.2010.32.018.
[33] A.O. Al-Sulttani, A. Ahsan, A. Rahman, N.N. Nik Daud, S. Idrus, Heat transfer coefficients and yield analysis of a double-slope solar still hybrid with rubber scrapers: An experimental and theoretical study, Desalination. 407 (2017) 61–74. https://doi.org/10.1016/j.desal.2016.12.017.
[34] A. Madhlopa, C.M. Johnstone, Computation of solar radiation distribution in a solar still with internal and external reflectors, Solar Energy. 85 (2011) 217–233. https://doi.org/10.1016/j.solener.2010.12.010.
[35] M. Sakthivel, S. Shanmugasundaram, Effect of energy storage medium (black granite gravel) on the performance of a solar still, International Journal of Energy Research 32 (2008) 68–82. https://doi.org/10.1002/er.1335.
[36] S. Aboul-Enein, A.A. El-Sebaii, M.R.I. Ramadan, H.G. El-Gohary, Parametric study of a solar air heater with and without thermal storage for solar drying applications, Renewable Energy 21 (2000) 505–522. https://doi.org/10.1016/S0960-1481(00)00092-6.
[37] S. Trevisan, W. Wang, B. Laumert, Coatings utilization to modify the effective properties of high temperature packed bed thermal energy storage, Applied Thermal Engineering 185 (2021) 116414. https://doi.org/10.1016/j.applthermaleng.2020.116414.
[38] Correlation Coefficient | SpringerLink, (n.d.). https://link.springer.com/referenceworkentry/10.1007/978-0-387-79061-9_707 (accessed November 12, 2023).
[39] K.J. Khatod, V.P. Katekar, S.S. Deshmukh, An evaluation for the optimal sensible heat storage material for maximizing solar still productivity: A state-of-the-art review, Journal of Energy Storage 50 (2022) 104622. https://doi.org/10.1016/j.est.2022.104622.